DRAFT VERSION JANUARY 18, 2022
Preprint typeset using LaTeX style emulateapj v. 11/26/03

DISK GALAXY FORMATION IN A ΛCDM UNIVERSE

BRANT ROBERTSON[1,4], NAOKI YOSHIDA[2], VOLKER SPRINGEL[3], AND LARS HERNQUIST[1]

Draft version January 18, 2022

ABSTRACT

We describe hydrodynamical simulations of galaxy formation in a Λ cold dark matter (CDM) cosmology performed using a subresolution model for star formation and feedback in a multiphase interstellar medium (ISM). In particular, we demonstrate the formation of a well-resolved disk galaxy. The surface brightness profile of the galaxy is exponential, with a *B*-band central surface brightness of 21.0 mag arcsec^{-2} and a scale-length of $R_{\rm d} = 2.0\,h^{-1}$kpc. We find no evidence for a significant bulge component. The simulated galaxy falls within the *I*-band Tully-Fisher relation, with an absolute magnitude of $I = -21.2$ and a peak stellar rotation velocity of $V_{\rm rot} = 121.3\,{\rm km\,s^{-1}}$. While the total specific angular momentum of the stars in the galaxy agrees with observations, the angular momentum in the inner regions appears to be low by a factor of ~ 2. The star formation rate of the galaxy peaks at ~ 7 M$_\odot$ yr^{-1} between redshifts $z = 2-4$, with the mean stellar age decreasing from ~ 10 Gyrs in the outer regions of the disk to ~ 7.5 Gyrs in the center, indicating that the disk did not simply form inside-out. The stars exhibit a metallicity gradient from 0.7 Z$_\odot$ at the edge of the disk to 1.3 Z$_\odot$ in the center. Using a suite of idealized galaxy formation simulations with different models for the ISM, we show that the effective pressure support provided by star formation and feedback in our multiphase model is instrumental in allowing the formation of large, stable disk galaxies. If ISM gas is instead modeled with an isothermal equation of state, or if star formation is suppressed entirely, growing gaseous disks quickly violate the Toomre stability criterion and undergo catastrophic fragmentation.

Subject headings: galaxies: evolution – galaxies: formation – methods: numerical

1. INTRODUCTION

Numerical simulations have become one of the most important theoretical tools for exploring the complicated problem of galaxy formation. Modern numerical work on galaxy formation was initiated by Katz & Gunn (1991), Navarro & Benz (1991), and Katz (1992), who included radiative cooling by hydrogen and helium, and attempted to account for star formation and feedback processes. Subsequent work employed more sophisticated treatments of supernova feedback (Navarro & White 1993), models for chemical enrichment (Steinmetz & Müller 1994), and methods to 'zoom in' on galaxies of interest within cosmological simulations (Navarro & White 1994)

While these studies achieved limited success in creating rotationally supported disks, the simulated galaxies typically failed to reproduce their observed counterparts. In general, the simulated disks were found to be too small and were more centrally concentrated than actual galaxies (Navarro & White 1993, 1994; Navarro et al. 1995). In addition, the star formation in the models was overly efficient, converting too large a fraction of the gas into stars by the present day (Navarro et al. 1995; Steinmetz & Müller 1994, 1995).

Many of the shortcomings of the early modeling can be tied to the coarse resolution of the simulations and the manner in which feedback was treated. In a cosmological context, the multiphase structure of the ISM within galaxies cannot be resolved in detail, so star-forming gas is generally described as a single-phase medium. If feedback energy is deposited into this gas purely as thermal energy, it will be quickly radiated away, and any impact of feedback from star formation will be lost. In addition, if star formation is very efficient in low mass halos at high redshifts, a large number of dense, compact galaxies will form and eventually be incorporated into the inner regions of larger galaxies through hierarchical merging. If these baryonic clumps lose angular momentum to dark halos, the resulting objects will be smaller in extent than if the baryons had been accreted smoothly. Thus, an early collapse of baryons opens a channel for gas to lose angular momentum, yielding galaxies that are too compact, lack angular momentum, and produce stars overly efficiently compared with observations.

Subsequent work attempted to alleviate these shortcomings by employing stronger forms of feedback and modifications to the cosmological framework. In some cases, the problems noted above were exacerbated. For example, photoheating by a diffuse ultraviolet (UV) background was found to further reduce the angular momentum content of the simulated galaxies (Navarro & Steinmetz 1997). Other efforts included the impact of preheating and gas blow-out from small halos (Sommer-Larsen et al. 1999) and the formation of galaxies in a warm dark matter (WDM) cosmology (Sommer-Larsen & Dolgov 2001). More direct comparisons to observations were made possible by incorporating spectral synthesis techniques into the modeling (Contardo et al. 1998) and by using the Tully-Fisher relation to constrain the hierarchical origin of galaxies (Steinmetz & Navarro 1999; Navarro & Steinmetz 2000). However, the galaxies in these simulations were still too concentrated.

The most recent studies of disk formation have yielded somewhat more promising results. Using a model of self-propagating star formation combined with supernova feedback and a UV background, Sommer-Larsen et al. (2002, 2003) produced disk galaxies deficient in angular momentum by less than an order of magnitude. Governato et al. (2002)

[1] Harvard-Smithsonian Center for Astrophysics, 60 Garden St., Cambridge, MA 02138, USA
[2] National Astronomical Observatory Japan, Osawa 2-21-1, Mitaka, Tokyo 181-8588, Japan
[3] Max-Planck-Institut für Astrophysik, Karl-Schwarzschild-Straße 1, 85740 Garching bei München, Germany
[4] brobertson@cfa.harvard.edu

report the formation of realistic disk galaxies in ΛCDM and ΛWDM cosmologies using simulations that include standard prescriptions for cooling, a UV background, and star formation. Abadi et al. (2003a,b) present detailed analyses of simulated galaxies with kinematic and photometric properties similar to observed Sab galaxies.

Although the various attempts to simulate disk formation have provided some impressive successes, the essential physics behind this process remains unclear. Governato et al. (2002) claim that the low angular momentum of simulated galaxies in previous works owed at least partly to inadequate resolution. In addition, they emphasize the impact that the matter power spectrum can have on galaxy formation through simulations of WDM universes in which the bulge and spheroid components of galaxies are smaller than in CDM models. These findings are supported by Sommer-Larsen et al. (2002, 2003) and Sommer-Larsen & Dolgov (2001), whose calculations indicate that high resolution, strong stellar feedback, and warm dark matter can produce realistic disk galaxies. Finally, Abadi et al. (2003a) suggest that a crucial ingredient for forming proper disks is an implementation of feedback that can regulate star formation.

Here, we use a 'multiphase model' to describe star-forming gas, in which the ISM consists of cold clouds in pressure equilibrium with an ambient hot phase (Springel & Hernquist 2003a). Radiative cooling of gas leads to the growth of clouds, which in turn host the material that fuels star formation. The supernovae associated with star formation provide feedback by heating the ambient medium and evaporating cold clouds. The feedback treatment establishes a self-regulated cycle for star formation, pressurizing the star-forming gas. Implemented in a subresolution manner, our approach makes it possible to obtain numerically converged results for the star formation rate at moderate resolution. This feature is particularly important for simulations of CDM cosmologies, where early generations of galaxies may be difficult to resolve.

Using this model of star-forming gas, Springel & Hernquist (2003b) obtained a converged prediction for the history of cosmic star formation that agrees well with observations at redshifts $z \leq 4$ (Springel & Hernquist 2003b; Hernquist & Springel 2003).[1] In subsequent work, Nagamine et al. (2003a,b,d) showed that this model also accounts for the observed abundance and star formation rates of damped Lyman-alpha absorbers and Lyman-break galaxies at $z \sim 3$.

In what follows, we study the consequences of our multiphase model for the ISM on the formation of disk galaxies. First, we employ a high-resolution simulation to identify realistic disk galaxies in a cosmological context. For one such disk galaxy, we examine its kinematic and photometric properties in detail, demonstrating good agreement with observations of local spirals. Second, we use a set of idealized simulations to study disk formation in individual dark matter halos to isolate the effect of different models for the equation of state of the ISM. This analysis demonstrates that the feedback in our multiphase model alters the dynamics by pressurizing the star-forming gas and stabilizing forming disks against fragmentation. We emphasize that this aspect of our modeling does not depend on the details of our prescription for star formation and feedback, but is determined by the effective equation of state for star-forming gas. Thus, our conclusions should obtain generally, provided that the actual bulk equation of state for the ISM has characteristics similar to those of our description.

In § 2, we present our simulation method. We review our analysis procedure in § 3, and discuss our findings for the structural (§ 4) and kinematic properties (§ 5) of one simulated disk galaxy. In § 6, we describe our idealized simulations and their results. Finally, we conclude and suggest directions for further research in § 7.

2. COSMOLOGICAL SIMULATION

Our simulations were performed using the parallel *N*-body/smoothed particle hydrodynamics (SPH) code GADGET2 in its "conservative entropy" formulation (Springel & Hernquist 2002), to mitigate problems with lack of energy and entropy conservation in older treatments of SPH (e.g. Hernquist 1993; O'Shea et al. 2003). We adopt a flat ΛCDM cosmology with cosmological parameters $\Omega_{\rm m} = 0.3$, $\Omega_\Lambda = 0.7$, $\Omega_{\rm b} = 0.04$, and $\sigma_8 = 0.9$, and set the primordial power spectrum index to $n = 1$. Throughout, we select a value for the Hubble constant of $H_0 = 100\,h\,{\rm km\,s^{-1}Mpc^{-1}}$ with $h = 0.7$.

For our cosmological simulation, we populate a periodic volume of 10 h^{-1}Mpc on a side with 144^3 low-resolution dark matter (LRDM) particles. At the center of the box, a 5 h^{-1}Mpc cubic region is selected as a high resolution region where we replace the LRDM particles with particles of eight-times lower mass. The initial displacement field is then calculated following a standard "zooming" procedure (Tormen 1997; Power et al. 2003), where small scale perturbations are added appropriately in the high-resolution region. Note that the high-resolution zone does not target a particular object, with the intent of eliminating bias that could be introduced by selecting halos that may be intrinsically favorable for disk galaxy formation. We further split the high-resolution particles into dark matter (HRDM) and gas. The resulting particle masses of each component are then $m_{\rm LRDM} = 2.79 \times 10^7 h^{-1} M_\odot$, $m_{\rm HRDM} = 3.02 \times 10^6 h^{-1} M_\odot$, and $m_{\rm gas} = 4.65 \times 10^5 h^{-1} M_\odot$. We set the gravitational softening length for the high-resolution particles to 0.65 comoving h^{-1}kpc. While our 10 h^{-1} Mpc box is too small to be fully representative of the $z = 0$ universe, the volume is sufficient for our purposes as our current work does not concern, for example, large-scale correlations of galaxies or the global mass function. Here, we are interested only in individual, galactic-sized objects which are mostly unaffected by the simulation box size.

We include a UV background and radiative cooling and heating in the manner of Katz et al. (1996) and Davé et al. (1999), as well as star formation, supernova feedback, and metal enrichment. We employ the multiphase model developed by Springel & Hernquist (2003a) to describe the star-forming gas (see also Yepes et al. 1997; Hultman & Pharasyn 1999). Our approach accounts for some of the key aspects of the multiphase structure of the ISM (McKee & Ostriker 1977) without spatially resolving the different phases explicitly. Instead, a statistical mixture of the phases is computed analytically, taking into account the growth of cold clouds embedded in a supernova-heated ambient phase, the formation of stars

[1] We note an error in figure 12 of Springel & Hernquist (2003b) where the observational estimates of the star formation rate are plotted too high by a factor of $h^{-1} = 1.4$. When corrected, the observed points are in better agreement with the theoretical estimates; see astro-ph/0206395 and Nagamine et al. (2003c).

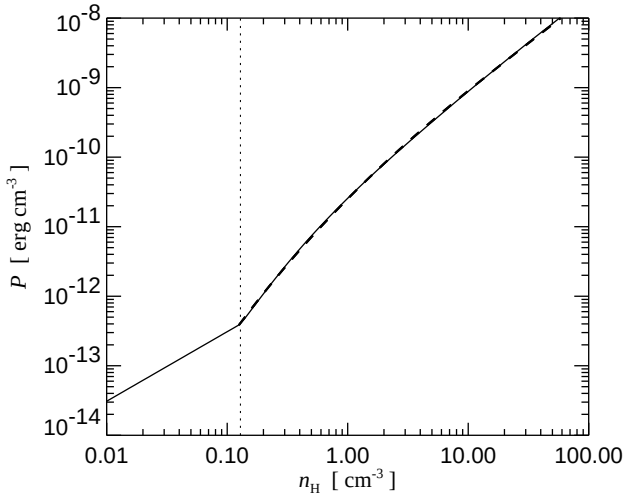

FIG. 1.— Effective equation of state for star-forming gas in our multiphase model (Springel & Hernquist 2003a). The effective pressure, $P_{\rm eff}$, is plotted in cgs units versus the total gas density in hydrogen atoms per cubic centimeter. The solid line is the exact equation of state, while the thick dashed line is a simple fit (see text), which is accurate to about 1%. The vertical dotted line shows the transition between an isothermal gas (to the left) and the effective equation of state in our multiphase model (to the right).

out of the cloud material, and the evaporation of clouds in supernova remnants.

Our strategy is motivated by two basic limitations in modeling star formation on cosmological scales. First, there is no fundamental theory of this process. Second, large-scale simulations lack the resolution that would be required to characterize the ISM in detail. Our statistical method decouples our ignorance of star formation from its impact on galactic scales, by coarse-graining the physics of star-forming gas. In principle, this strategy could be applied to any model of star formation.

For a detailed description of our multiphase model we refer the reader to Springel & Hernquist (2003a). For definiteness, we list in Table 1 the parameter values adopted in our simulations. The parameters include the efficiency of the evaporation process A_0, the mass fraction of stars that are short-lived and die as supernovae β, the cold gas cloud temperature $T_{\rm cloud}$, the effective supernova temperature $T_{\rm SN}$, and the gas consumption time-scale $t_0^\star$. As Springel & Hernquist (2003a) argue, all of these aside from one, e.g. $t_0^\star$, can be constrained by simple physical arguments. We adjust $t_0^\star$ to match the Kennicutt Law which describes empirically observed star formation rates in nearby galaxies (e.g. Kennicutt 1989, 1998).

On the surface, our description of star-forming gas appears complicated, with the properties of the different phases described by differential equations that include the various processes listed above. However, in the end, our model can be reduced to two main ingredients that make our results easier to interpret. Springel & Hernquist (2003a) showed that the star-forming gas quickly establishes a self-regulated cycle in which the mass and energy of the phases can be approximated by equilibrium solutions. In this limit, the impact of star formation and feedback can be reduced to: 1) the rate at which gas is converted into stars, and 2) the effective equation of state for star-forming gas.

Here, as in Springel & Hernquist (2003a), we choose to parameterize the star formation rate by

$$\frac{{\rm d}\rho_*}{{\rm d}t} = (1-\beta)\frac{\rho_c}{t_*}, \qquad (1)$$

where

$$t_* = t_0^\star \left(\frac{\rho}{\rho_{\rm th}}\right)^{-1/2}. \qquad (2)$$

The free parameter $t_0^\star$ is chosen to match the Kennicutt Law, $\rho_{\rm th}$ is a threshold density above which gas is subject to thermal instability and star formation, and ρ_c is the density of clouds which, in equilibrium, is given by equation (18) of Springel & Hernquist (2003a). Springel & Hernquist (2003a) showed that $\rho_{\rm th}$ can be fixed by e.g. requiring the equation of state to be continuous.

In our subresolution model, feedback from supernovae adds thermal energy to the ISM, pressurizing it and modifying its equation of state. On the scales relevant to the dynamics of the gas, this is described by an effective equation of state, which can be written

$$P_{\rm eff} = (\gamma-1)\,\rho\,u_{\rm eff}, \qquad (3)$$

where γ is the ratio of specific heats, ρ is the total gas density, and $u_{\rm eff}$ is the effective specific thermal energy of the star-forming gas which, in equilibrium, is given by equation (19) of Springel & Hernquist (2003a). The effective equation of state for the particular model parameters employed in our study is illustrated in Figure 1, in cgs units. Also shown in Figure 1 is a simple fit to the equation of state, which is accurate to about 1% and is given by

$$\log P_{\rm eff} = 0.050(\log n_{\rm H})^3 - 0.246(\log n_{\rm H})^2 + 1.749\log n_{\rm H} - 10.6, \ \text{for } \log n_{\rm H} > -0.89. \qquad (4)$$

In the particular example shown in Figure 1, the gas is assumed to be isothermal for densities $\rho \le \rho_{\rm th}$. In cgs units, for the parameter choices adopted here, the critical density at which the gas begins to depart from isothermality is $n_{\rm H,th} = 0.128$ cm^{-3}. This choice ensures that the effective pressure is a continuous function of density. For the equation of state shown in Figure 1, a different value of $n_{\rm H,th}$ would introduce an unphysical jump in pressure at the transition density where the gas is no longer isothermal.

Our implementation of feedback differs significantly from previous works (e.g. Sommer-Larsen et al. 2003; Governato et al. 2002). In our subresolution model, feedback energy is "stored" in the surrounding gas, adding pressure support to it. As shown in Figure 1, at densities $\rho > \rho_{\rm th}$, the equation of state becomes stiffer than isothermal due to this feedback energy. This pressurization regulates star formation occurring within the ISM and, as we discuss later, modifies the bulk dynamics of the gas by altering the pressure gradient term in Euler's equation. It is this property of our description that we believe is responsible for many of the differences between our numerical results and earlier simulations.

TABLE 1. SPRINGEL & HERNQUIST (2003A) MODEL PARAMETERS

Parameter	Symbol	Value
Supernova Evaporation	A_0	1000
Mass Fraction of Stars $> 8M_\odot$	β	0.1
Cold Cloud Temperature	$T_{\rm clouds}$	1000 K
Effective Supernova Temperature	$T_{\rm SN}$	10^8 K

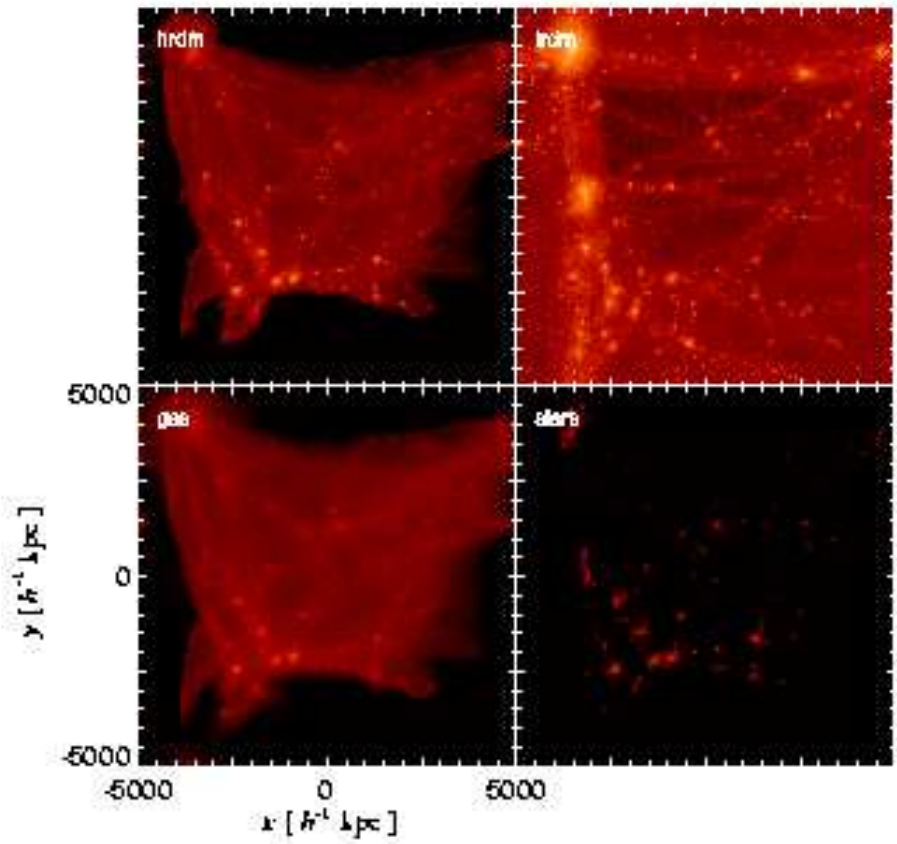

FIG. 2.— Entire simulation volume at $z = 0$ projected onto a 10 h^{-1} Mpc square area, showing the end-state of the simulation. The upper left and right panels show the HRDM and LRDM particles, respectively. The lower left and right panels show the gas and star particles, respectively. Owing to gravitational effects the low- and high-resolution particles have intermingled at the boundary of the high-resolution region, but the LRDM particles have not penetrated the inner high-resolution region. Star particles have spawned in regions where the gas density has exceeded the critical density for star formation.

In passing, we note that for the purposes of large-scale dynamics, our multiphase model can be reduced to the choice of star formation rate, e.g. equation (1), and the effective equation of state of star-forming gas, e.g. equation (5) and Figure 1. The results presented here could be obtained with any hydrodynamical code that uses the same expression for the star formation rate and an equation of state like that in Figure 1, without specific reference to all the complexities of our multiphase model.

In Figure 2, we show the evolved simulation volume at $z = 0$, in projection. The upper and lower left panels show the high-resolution dark matter (HRDM) and gas particles, respectively. The high-resolution region of the simulation has increased in size from the initial 5 h^{-1} Mpc cubic region at the center of the simulation, owing to the growth of gravitational structure. Some of the low- and high-resolution particles have mixed in the boundary region of the low-resolution zone, whose shape has also been distorted. However, the LRDM particles (upper right panel) have not penetrated into the inner regions of the high-resolution region where many luminous galaxies have formed out of the gas, as marked by the star particles (lower right panel).

3. DISK GALAXY SELECTION

We use a standard friends-of-friends (FOF) group-finding algorithm to identify dark matter halos, restricting ourselves to objects comprised of high-resolution particles. We then identify the most bound star or gas particle within each object and produce a new collection of particles for each halo that encompasses all particles that lie within the radius R_{200} that encloses 200 times the critical density around these most-bound baryonic particles. The group catalogue produced from this procedure serves as our primary galaxy sample.

From our galaxy catalogue, we have visually inspected the 10 largest objects, measured their angular momenta, and selected a large disk galaxy for further detailed analysis in this paper. This galaxy displays the most disk-like morphology of all the galaxies in the simulation resolved with a similar number of particles. While we do find other flattened systems in the simulation, the majority of them do not display such well defined disk-like morphology and kinematics as the galaxy described below.

The galaxy analyzed here, which we term "galaxy C1" for simplicity, has 61,372 dark matter, 21,506 gas, and 88,138 star particles within R_{200} at $z = 0$. Note that the star particle mass was set to half the original mass of the gas particles, so the overall baryon fraction within R_{200} is 14.1%; slightly larger than the universal baryon fraction of 13.3%. Figure 3 shows the star (left panels) and gas (right panels) particle distributions within $0.1\,R_{200}$ at $z = 0$, projected perpendicular (upper panels) and parallel (lower panels) to the direction of the stellar angular momentum. In addition, the lower right

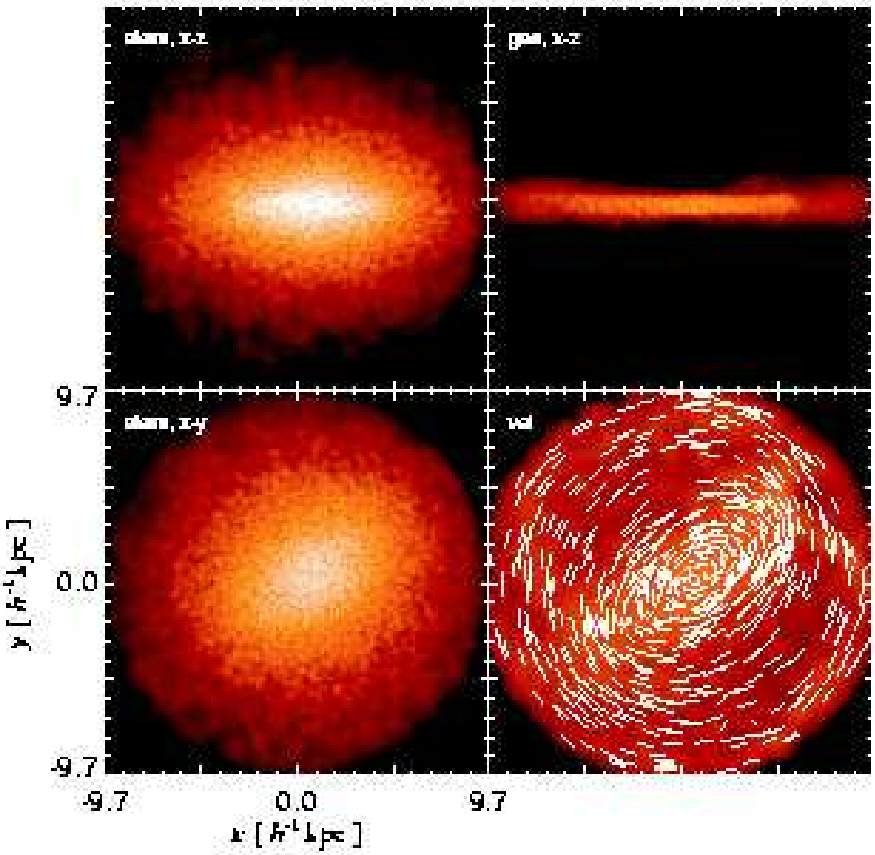

FIG. 3.— Disk galaxy at $z = 0$, displaying the star (left panels) and gas (right panels) particle distributions within $0.1\,R_{200}$, projected perpendicular (upper panels) and parallel (lower panels) to the direction of the stellar angular momentum vector. The lower right panel also traces the gas velocity field and demonstrates the rotational support of the galaxy.

panel traces the gas velocity field in the plane of the disk. The gas in the galaxy has collapsed into a rotationally supported disk, surrounded by a thicker stellar disk. The velocity field of the galaxy illustrates the mainly circular trajectories of the gas particles in the disk plane. A weak bar is visible in the disk gas, but is not strong in the stars that dominate the baryonic mass of the galaxy. We note that the stellar component is slightly elongated in the direction of the bar, however. The galaxy has reached a mass of $M_{200} = 2.16 \times 10^{11} h^{-1}$ M$_\odot$ at $z = 0$, with a stellar mass of $M_\star = 2.05 \times 10^{10} h^{-1}$ M$_\odot$ and a gas mass of $M_{\rm gas} = 9.44 \times 10^9 h^{-1}$ M$_\odot$. The baryonic mass of the galaxy is then 68% stellar and 32% gaseous.

4. STRUCTURAL PROPERTIES OF GALAXY C1

4.1. *Mass surface density profiles*

Figure 4 shows the stellar (diamonds) and gas (triangles) mass surface densities of galaxy C1 projected along the stellar angular momentum vector onto the disk plane. The stellar profile includes particles within $30\,h^{-1}$ kpc of the disk center, while the gas profile includes particles only within $2\,h^{-1}$ kpc of the disk plane. The stellar and gas mass surface densities are roughly exponential out to $r = 8\,h^{-1}$ kpc. If we fit them with an exponential of the form

$$\Sigma(r) = \Sigma_0\, {\rm e}^{-r/R_d}, \qquad (5)$$

we find best fit values of $\Sigma_{0,\star} = 452\,h$ M$_\odot$pc^{-2}, $R_{\rm d,\star} = 2.3\,h^{-1}$kpc for the stars and $\Sigma_{0,\rm gas} = 15.3\,h$ M$_\odot$pc^{-2}, $R_{\rm d,gas} = 4.7\,h^{-1}$kpc for the gas. In the plot, we include least squares fits to the stellar and gas mass surface densities. For comparison, the stellar disk of the Milky Way has a scale-length $R_{\rm MW} \sim 3.5$ kpc, similar to the physical scale-length of ~ 3.3 kpc for our simulated galaxy C1. We note that the gas mass surface density begins to diverge from the exponential fit between $8 - 10\,h^{-1}$ kpc, at the edge of the gaseous disk.

4.2. *Photometric properties*

From the known masses, metallicities, and ages of the star particles, we use a population spectral synthesis code to calculate the SDSS *ugriz* (Fukugita et al. 1996) AB system magnitudes and *JHK* magnitudes for each particle. The population synthesis code assumes a Kroupa (2001) IMF and limits input metallicities to a range of $0.005\ {\rm Z}_\odot < {\rm Z} < 2.5\ {\rm Z}_\odot$, outside of which we adopt the minimum or maximum value. We then use the Fukugita et al. (1996) conversions from SDSS colors to the Johnson-Morgan-Cousins *UBVRI* (Johnson & Morgan 1953; Cousins 1978) Vega system to calculate the absolute magnitude of the star particles in each band. We bin star particles within $30\,h^{-1}$ kpc of the center of the galaxy into annuli and calculate their total luminosities to determine a surface brightness profile. The measured surface brightness of galaxy C1 in *B*, *V*, *I*, and *K*-bands is plotted in Figure 5. The best fit *B*-band central surface brightness is $\mu_{0,B} = 21.0$ mag arcsec^{-2} with a *B*-band luminosity scale-length of $R_{d,B} = 2.0$

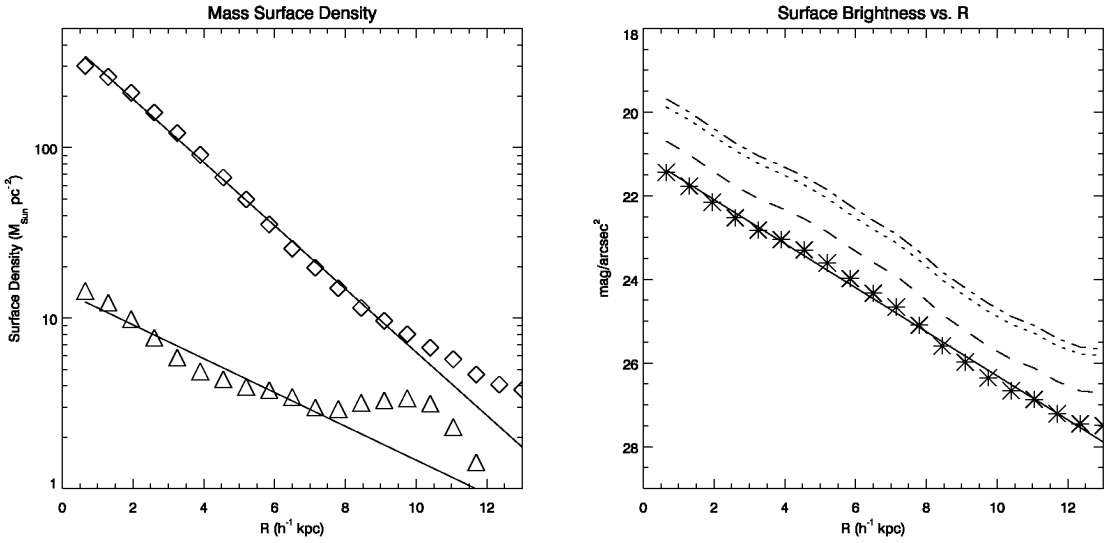

FIG. 4.— Mass surface density for the stars (diamonds) within $30h^{-1}$ kpc of the galaxy center and gas particles (triangles) within $2h^{-1}$ kpc of the disk plane. Using an exponential profile $\Sigma(r) = \Sigma_0 \exp(-r/R_d)$ to fit each component separately, we find best fit values of $\Sigma_{0,\star} = 452h$ $M_\odot pc^{-2}$, $R_{d,\star} = 2.3h^{-1}$kpc for the stars and $\Sigma_{0,\mathrm{gas}} = 15.2h$ $M_\odot pc^{-2}$, $R_{\mathrm{gas}} = 4.7h^{-1}$kpc for the gas. The least squares fit for the stars (solid line) and gas (dashed line) are plotted over the measured values.

FIG. 5.— Surface brightness profile of the galaxy in *B* (stars), *V* (dashed line), *I* (dashed-dotted line), and *K* (dotted line) bands. The solid line is the fit to the B-band profile, with best fit central surface brightness $\mu_{0,B} = 21.0$ mag arcsec^{-2} and B-band disk scale length $R_{d,B} = 2.0h^{-1}$ kpc. The standard central B-band surface brightness value for disk galaxies is $\mu_{B,\mathrm{Freeman}} = 21.65$ mag arcsec^{-2}. The disk brightness is exponential in each band throughout the inner 10 h^{-1} kpc of the galaxy.

h^{-1} kpc. Our measured value for the *B*-band central surface brightness agrees well with the canonical value of $\mu_{0,B} = 21.65$ mag arcsec^{-2} for spiral galaxies (Freeman 1970).

Figure 5 demonstrates that the surface brightness profile of galaxy C1 is exponential from the very center of the galaxy out to $r \sim 10h^{-1}$ kpc, and shows no evidence for a bulge component. To our knowledge, this object is the first published example of a galaxy formed within a cosmological simulation that displays an exponential surface brightness profile with no significant bulge.

For reference, the *u*, *g*, *v*, *r*, *i*, *z*, *U*, *B*, *R*, *I*, *J*, *H*, and *K*-band absolute magnitudes of the galaxy, measured by summing the luminosities of all stars used to calculate the surface brightness profiles out to 25.0 mag arcsec^{-2} in each band, are listed in Table 2. The galaxy has realistic colors, and its properties agree with recent 2MASS determinations of $B-K$ vs. M_K color measurements of nearby spiral galaxies (J. Huchra 2003, private communication). We also list the stellar mass-to-light ratios Υ_x in each band, for comparison with observed galaxies. The stellar mass-to-light ratios in the *g*, *r*, *i*, and *z* bands agree well with the properties of observed galaxies in the Sloan survey (Kauffmann et al. 2003).

4.3. *Star and metal formation histories*

Within our simulation code, we record the formation time of each star particle, allowing us to infer the detailed star formation history of each object. Similarly, the metallicity of the star particles can be used to determine the metallicity evolution of the galaxies. Figure 6 shows the star formation history of galaxy C1. As a function of redshift (left panel), the star formation rate rises below redshift $z = 10$ and peaks at a value ~ 7 $M_\odot$ yr^{-1} at redshift $z \sim 3$, after which it declines sharply to the present time. In the right panel of Figure 6, we also plot the star formation rate against lookback time. Viewing the star formation history in this way illustrates that most of the stars formed early on, with the majority of stars in the galaxy at $z = 0$ being older than 9 billion years. A large fraction of these stars formed in progenitor halos that later merged to form the galaxy.

Figure 7 illustrates the history of the metal content of the galaxy. Each panel shows the average metallicity of newly formed stars (solid line) over the lifetime of the galaxy and the average metallicity of all stars formed before each epoch (dashed line). While the metallicity of newly formed stars varies in a complex manner, reflecting the details of gas accretion and merging, the average metallicity of the galaxy evolves smoothly to the current epoch. The large feature at $z = 0.8$ corresponds to a major merger in the assembly history of the galaxy that significantly altered the metallicity between $z = 0.7$ and $z = 0.5$. Note that stars formed before 9 billion years ago have average metallicities of < 0.8 $Z_\odot$. We hence expect to see an older population of relatively metal-poor stars, while regions of the galaxy that actively formed stars even at late times should feature a younger, metal-rich population. If a disk does not form stars at the same rate everywhere, we would expect to see stellar age and metallicity gradients between regions of differing star formation activity.

4.4. *Stellar age and metallicity gradients*

Combining the formation time and metallicity of each star particle with information about its position allows us to determine stellar age and metallicity gradients in the galaxy. The left panel of Figure 8 shows the stellar age gradient in the disk, measured for all star particles within $15h^{-1}$ kpc from the center of the galaxy. The average age of the star particles decreases from ~ 10 Gyr in the outer regions of the disk to ~ 7.5 Gyr in the center. Beyond a radius of $\sim 10h^{-1}$ kpc, the average age of the stars is dominated by contributions from the stellar halo, where stars are significantly older than in the disk.

TABLE 2. PHOTOMETRIC PROPERTIES OF GALAXY C1

Band	*u*	*g*	*r*	*i*	*z*	*U*	*B*	*V*	*R*	*I*	*J*	*H*	*K*
Magnitude	-18.1	-19.7	-20.4	-20.7	-20.9	-19.1	-19.3	-20.1	-20.6	-21.2	-21.1	-21.3	-21.0
Υ_X	12.3	3.23	1.85	1.45	1.19	5.88	4.95	2.40	1.52	0.91	0.98	0.84	1.07

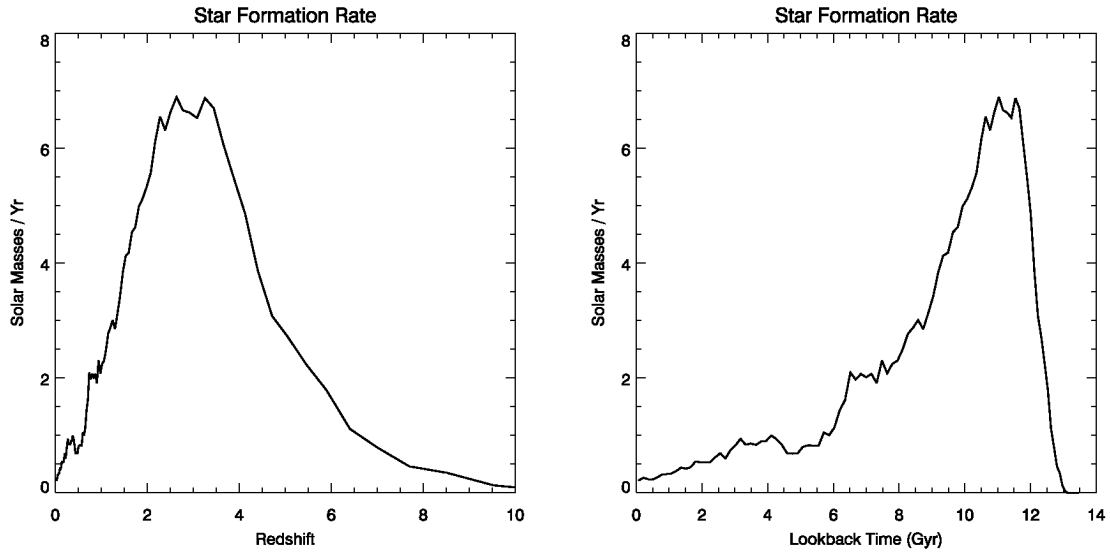

FIG. 6.— Star formation history of the entire simulated galaxy as a function of redshift (left panel). The star formation rate in the galaxy increases from redshift $z = 10$ to a peak of $\sim 7\ M_\odot\ yr^{-1}$ at $z \sim 3$. The right panel shows the galactic star formation history as a function of lookback time. Most of the stars in the galaxy formed earlier than 9 Gyr ago.

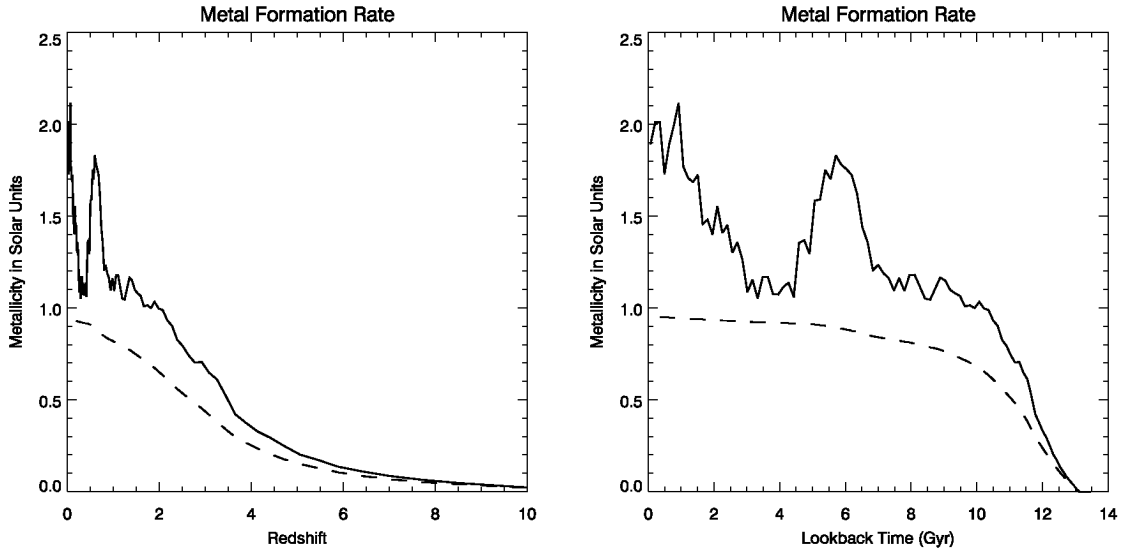

FIG. 7.— Metal formation history of the simulated galaxy. In each panel, the solid line shows the average mass-weighted metallicity of newly formed stars over the lifetime of the galaxy. The dashed line shows the running mass-weighted average metallicity of all stars within the galaxy. The left panel is plotted as a function of redshift and the right panel is plotted against lookback time. The large feature at $z = 0.8$ corresponds to a major merger in the assembly history of the galaxy that significantly altered the metallicity between $z = 0.7$ and $z = 0.5$.

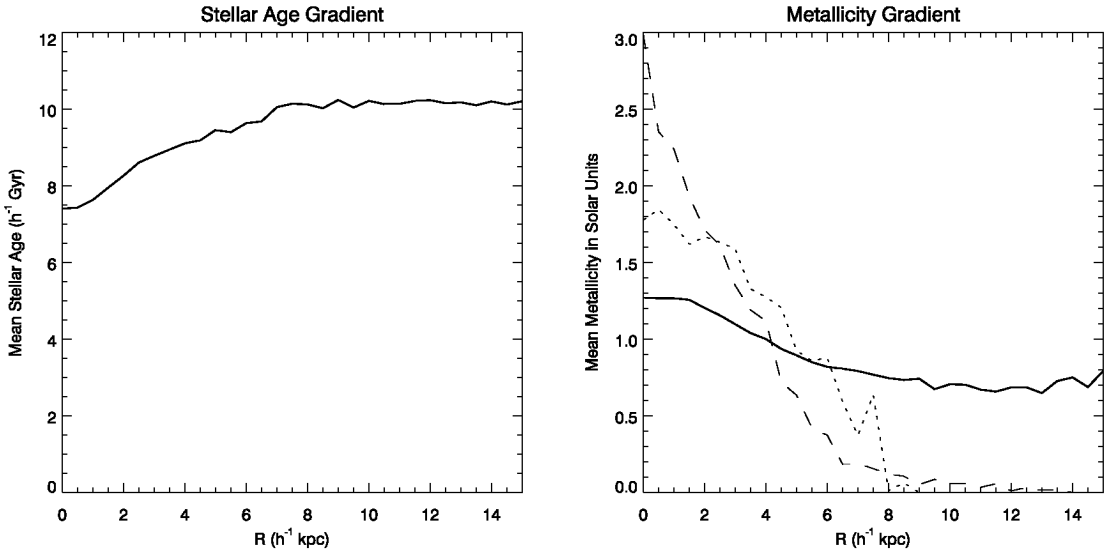

FIG. 8.— Stellar age gradient in the disk (left panel), measured by averaging the ages of star particles in $0.5h^{-1}$kpc radial bins. The average age of the stars decreases from ~ 10 Gyr in the outer regions of the disk to ~ 7.5 Gyr in the center. The right panel shows the stellar (solid) and gas (dashed) metallicity gradients in the disk. The metallicity of the stars increases from ~ 0.75 $Z_\odot$ at the edge of the disk to ~ 1.3 $Z_\odot$ in the center, while that of the gas in the disk increases strongly from primordial values in the outer disk to ~ 2.5 $Z_\odot$ in the central regions. Stars forming after $z = 0.25$ (dotted line) track the metallicity gradient of star-forming gas in the disk.

In the right panel of Figure 8 we show the metallicity gradient in the galaxy, plotting the average metallicity of the star (solid line) and gas (dashed line) components in $0.5h^{-1}$ kpc radial bins. The metallicity gradient of the stars tracks the stellar age gradient closely, remaining at a roughly constant value of ~ 0.7 $Z_\odot$ from $r = 15h^{-1}$ kpc to $r = 8h^{-1}$ kpc and then increasing to a central value of Z= 1.3 $Z_\odot$. Again, the halo stars beyond $10h^{-1}$kpc are older and deficient in metals compared with the younger stars in the disk. Interestingly, the gas metallicity gradient is much stronger than the stellar metallicity gradient, increasing from close to primordial values at $r = 8h^{-1}$ kpc to ~ 2.6 $Z_\odot$ near the center of the disk. The gas in the inner regions has been enriched by stars forming at late times (dotted line, for stars forming after $z = 0.25$), whose metallicities have been enhanced by the long history of star formation in the galaxy. The metallicity gradients of the star-forming gas and recently formed stars in the disk then track each other, again highlighting the strong metallicity gradient in the gaseous disk.

The active star formation in the disk produces a collection of stars that are younger and more metal enriched than in the outer regions of the galaxy. Hence, the disk is not simply built up inside-out, but instead partially forms outside-in (Sommer-Larsen et al. 2003). The more active star formation at late times in the inner disk makes this region actually quite young, on average. In the halo of the galaxy, where star formation is dormant, stars are significantly older and more metal poor than in the disk.

5. KINEMATIC PROPERTIES OF GALAXY C1

5.1. *Angular momentum*

Perhaps the most important kinematic property of disk galaxies is their angular momentum, as this quantity determines the sizes of thin, rotationally supported disks (Mo et al. 1998). While measuring the specific angular momentum $j_\star$ of each star particle is straightforward, deciding which particles to use for measuring the angular momentum content of the disk is less clear, in particular when comparing with observations.

We wish to compare our simulated galaxy with the *I*-band Tully-Fisher relation measured by Mathewson et al. (1992) and Courteau (1997) and the corresponding $j_\star - V_{\rm rot}$ relation (as compiled by Navarro 1998). The measured rotation velocity $V_{\rm rot}$ used for these relations is determined observationally at 2.2 times the exponential scale-length of the stellar surface brightness, R_d. We then take $V_{\rm rot}$ to be

$$V_{\rm rot} = \sqrt{\frac{GM(<R_V)}{R_V}}, \tag{6}$$

$$R_V = 2.2R_{d,B}, \tag{7}$$

where $R_{d,B}$ is the *B*-band surface brightness scale-length determined in § 4.2. In what follows, when we refer to $V_{\rm rot}$ we always mean the expected rotation velocity corresponding to the circular velocity produced by all mass within $2.2 \times R_{d,B} = 0.045R_{200}$ for galaxy C1.

Having determined the rotation velocity $V_{\rm rot}$, we then consider 3 different approaches for measuring the specific stellar angular momentum $j_\star$, providing slightly different interpretations of the angular momentum content of the galaxy. For all the star particles, we define the total specific stellar angular momentum $j_{\star,\rm tot}$ to be a sum over the star particles of the form

$$j_{\star,\rm tot} = \left| \sum_{i=1}^{N_\star} m_i \mathbf{r}_i \times \mathbf{v}_i \right| \Bigg/ \sum_{i=1}^{N_\star} m_i, \tag{8}$$

where $N_\star$ is the total number of star particles within R_{200}, $\mathbf{v}_i$ is the velocity with respect to the center of mass of the galaxy, $\mathbf{r}_i$ is the distance from the center of the galaxy, and m_i is the mass of the $i^{\rm th}$ star particle.

We also consider the specific angular momentum $j_{\star,\rm R_V}$ of the stars within the radius R_V at which the rotation velocity is measured. This is determined by simply restricting the sums in equation (8) to the stars within a distance R_V of the center of the galaxy.

The final method we employ mimics the observational estimate for the specific angular momentum content of an expo-

nential disk, viz.

$$j_{\star,\rm obs} = 2\,R_{d,B}\,V_{\rm rot}. \quad (9)$$

Unlike the previous two methods, this technique indirectly estimates the angular momentum content by combining a measurement of the size of the disk with a typical circular velocity. While allowing an inter-comparison of observed galaxies with similar rotation velocities (Abadi et al. 2003a), this approach implicitly assumes that the disk has the rotation curve of an exponential disk (Courteau 1997), which is not true in general.

We summarize the angular momentum of our simulated galaxy in Table 3, listing the values for $V_{\rm rot}$ and the three different measurements of $j_\star$ along with their values in physical units. With a rotation velocity $V_{\rm rot} = 121.3\,{\rm km\,s^{-1}}$ and total specific stellar angular momentum $j_\star = 204.2\,h^{-1}$ kpc km s^{-1}, this galaxy agrees favorably with the observed range of $\log(j_\star) \sim 2.4-3.2$ for galaxies with $\log(V_{\rm rot}) \sim 2.1$ (Mathewson et al. 1992; Courteau 1997; Navarro 1998). However, the region of the galaxy within R_V has a specific angular momentum lower by a factor of ~ 2 with $j_{\star,R_V} = 101.0\,h^{-1}\,{\rm kpc\,km\,s^{-1}}$. The lower angular momentum of this part of the galaxy results from the thickness of the stellar disk. Finally, the agreement between the value $j_{\star,\rm obs} = 485.2h^{-1}$ kpc km s^{-1} and the observed range of $j_\star$ demonstrates that the stellar disk has the proper size when compared with observed galaxies of similar rotation velocity.

Overall, we find that the total angular momentum content of the galaxy is appropriate for its rotation velocity, when compared to observations, but that the thick disk reduces the specific stellar angular momentum content in the inner regions. We stress that the stellar disk of this galaxy should be considered deficient in angular momentum content and caution that only measuring the total specific stellar angular momentum content of a simulated galaxy can lead to an overestimate of the specific stellar angular momentum in the central regions of the galaxy.

At present, we cannot determine whether the low angular momentum in the inner regions of the galaxy is purely a physical effect, or is at least partly a consequence of our relatively poor spatial resolution. The gravitational softening length in the high-resolution region of our simulation is $0.65h^{-1}$ kpc. For $h = 0.7$, this means we cannot resolve thin stellar disks of galaxies like the Milky Way. It is possible that our estimate of the angular momentum of the inner parts of galaxy C1 is underestimated because of this problem.

5.2. *Rotation curve*

In Figure 9, we plot the rotation velocity of gas particles from within 2 h^{-1} kpc of the disk plane (crosses), projected onto 0.5 h^{-1} kpc wide annuli. We find that the rotation velocity of the gas closely traces the total rotation velocity $V(R) = [GM(<R)/R]^{1/2}$ (solid line), as expected for a thin disk without a dominant bulge component. If the central regions of the galaxy contained a kinematically important bulge, the gas rotation curve would either rise steeply or have a central maximum and decline outwards. We interpret the slowly rising rotation velocity of the gas as further evidence that galaxy C1 consists of a rotationally supported exponential disk without a significant bulge component.

TABLE 3. KINEMATIC PROPERTIES OF GALAXY C1

Method	Radius (h^{-1} kpc)	V_{rot} (km s^{-1})	$j_\star$ (h^{-1} kpc km s^{-1})	$\log(j_\star)$ $+\log(h_{70})$
Total	R_{200}	121.3	204.2	2.465
R_V	$2.2R_{d,B}$	121.3	101.0	2.159
"Observed"	$2R_{d,B}$	121.3	485.2	2.841

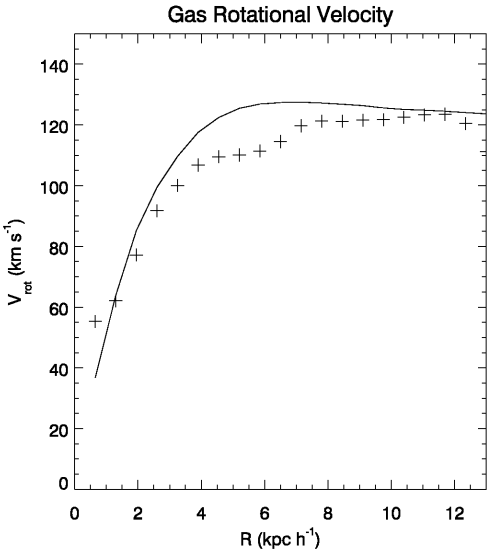

FIG. 9.— Rotation velocity of the gas particles within 2 h^{-1} kpc of the disk plane (crosses), projected onto 0.5 h^{-1} kpc annuli. We find that the gas rotation velocity closely traces the total rotation velocity $V(R) = [GM(<R)/R]^{1/2}$ (solid line), as expected for a thin disk without a dominant bulge component.

5.3. *I-band Tully-Fisher relation*

From the photometric modeling described in § 4.2 and the kinematic measurements in § 5.1, it is possible to compare galaxy C1 with the *I*-band Tully-Fisher relation as determined by Giovanelli et al. (1997), Han & Mould (1992), and Mathewson et al. (1992). For our measured *I*-band magnitude of $I = -21.2$ and rotation velocity $V_{\rm rot} = 121.3$ km s^{-1}, we find our galaxy to be in good agreement with the average observed *I*-band magnitude of $I \sim -20.8$ for galaxies with $\log(V_{\rm rot}) \sim 2.1$.

6. ISOLATED HALO SIMULATIONS

The formation of a well-defined disk galaxy without a dominant bulge can be viewed as a significant success towards obtaining realistic galaxies in cosmological simulations. It is therefore of particular interest to understand which aspects of our modeling are mainly responsible for this outcome.

A novel feature of our approach lies in our use of a subresolution model for the multiphase structure of the ISM, together with an effective equation of state that this model implies for the dense star-forming gas. As can be seen in Figure 1, when the gas is sufficiently dense to be thermally unstable and subject to star formation, the equation of state departs from that of an isothermal gas, and becomes stiffer with increasing density. This will affect the bulk hydrodynamics of the gas, through the pressure gradient term in the Euler equation. Consequently, dense gaseous disks will experience additional pressure support from supernova feedback, in a manner that is different from previous attempts to model galaxy formation.

In order to examine the importance of this effect further,

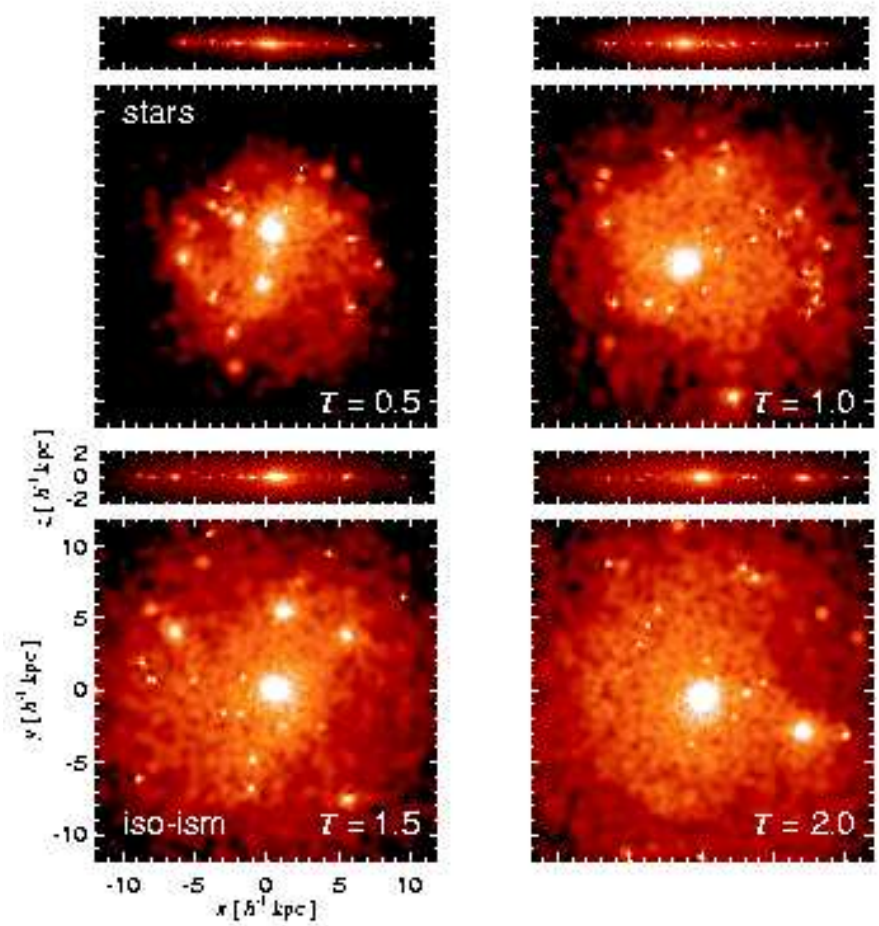

FIG. 10.— Stellar mass distribution, adaptively smoothed and seen edge- and face-on, for the "iso-ism" model at (clockwise from upper left) T = 0.5 Gyr, T = 1.0 Gyr, T = 1.5 Gyr, and T = 2.0 Gyr. As the disk develops, gas quickly cools to roughly 10^4 K and forms stars. The 10^4 K gas is Toomre unstable and fragments into dense clumps, which in turn efficiently form stars, leading to the clumpy stellar mass distribution in the disk. As the galaxy ages, the clumps lose angular momentum through dynamical friction, coalesce, and fall into the center of the galaxy.

we use a set of simulations to consider disks forming in isolated halos (e.g. Springel & Hernquist 2003a), where we vary the description of star-forming gas and associated feedback effects. These results show that the physics of dense, star-forming gas has a substantial impact on the dynamics of disks, indicating that the model of the ISM plays a crucial role in our successful formation of a disk galaxy in a cosmological context.

6.1. *Initial conditions and simulation set*

In order to isolate the dependence of disk formation on the physics of the ISM, we investigate the dynamics of gas in static spherically symmetric NFW (Navarro et al. 1995) dark matter halos of mass $10^{12}h^{-1}\ M_\odot$ and concentration $c_{\rm NFW} = 20$. We place 40,000 gas particles that initially trace the dark matter in these halos and set the initial temperature profile such that the gas is in hydrostatic equilibrium when evolved with non-radiative hydrodynamics. We add angular momentum to the gas, corresponding to a relatively high spin parameter of $\lambda = J|E|^{1/2}/(GM_{\rm vir}^{5/2}) = 0.1$. We then evolve the gas forward in time including radiative cooling. Under these conditions, we expect the gas to collapse smoothly into a thin, rotationally supported disk. We do not intend for this to be a realistic model of disk formation in a hierarchical universe, but the idealized nature of the simulations described below makes it possible to examine the consequences of varying the gas physics in detail.

This set-up provides initial conditions for a suite of simulations, where we consider three different descriptions of the ISM. The first model, which we will refer to as "justcool," consists of simply allowing the gas to cool with primordial abundances without allowing for any star formation or feedback. The "justcool" scenario serves as an extreme reference case where star formation and feedback cannot affect the gas dynamics. Since the dense gas that settles into a disk can cool efficiently, its temperature will remain close to 10^4 K, effectively obeying an isothermal equation of state.

Our second description of the ISM, which we refer to as "iso-ism," includes gas cooling and star formation, according to equation (1), but no feedback effects. Gas in the disk again obeys a nearly isothermal equation of state in this case, but compared to our "justcool" model, dense gas is converted into collisionless star particles. For ease of comparison, we use the same star formation rate for gas of a given density as in our multiphase model.

Finally, our third description of the ISM is the Springel & Hernquist (2003a) multiphase ISM model, which includes radiative cooling, star formation, and supernova feedback in the form of thermal energy input and cloud evaporation, as described earlier. We refer to this model as the "multiphase-ism" model. The primary difference between the "multiphase-ism" and "iso-ism" scenarios is that in the mul-

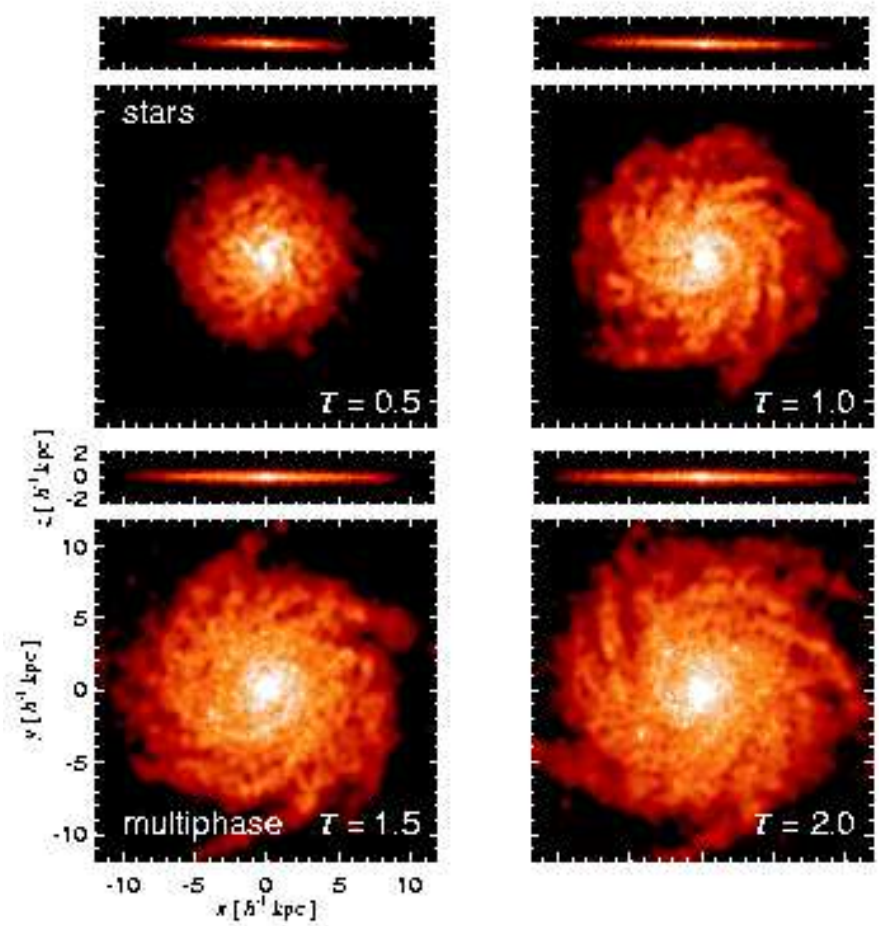

FIG. 11.— Stellar mass distribution, adaptively smoothed and seen edge- and face-on, for the "multiphase-ism" model at (clockwise from upper left) T = 0.5 Gyr, T = 1.0 Gyr, T = 1.5 Gyr, and T = 2.0 Gyr. In the "multiphase-ism" run, the gas cools into a thin disk which begins forming stars at a rate regulated by supernova feedback. While the gas is comprised of clouds cool enough to form stars, the contributions from the hot surrounding medium to the effective equation of state of the gas provides pressure support to the ISM to prevent Toomre instability. The end result is a large disk galaxy with only a modest bulge component.

tiphase model feedback from supernovae modifies the effective equation of state of star-forming gas, providing increased pressure support, as indicated by Figure 1. The stiffer equation of state helps to regulate star formation so that it occurs at a rate consistent with observations of isolated disk galaxies (Kennicutt 1989, 1998; Martin & Kennicutt 2001) once the free parameter $t_0^\star$ of the model is properly adjusted (see Springel & Hernquist 2003a,b).

For each ISM model, we ran a number of simulations, varying the numerical integration parameters to test the robustness of the results. In particular, we varied the number of SPH neighbors and the value of the time-step taken by the code. None of these choices had a significant effect on the outcome. Therefore, our results appear to have converged with respect to time integration. When the number of SPH neighbors is varied, instabilities in the disks tend to occur at slightly different times and locations, but the qualitative behavior of the simulations remains unchanged.

6.2. *Comparison of disks formed in isolated halos*

The time evolution of simulations with our three ISM models reveals interesting differences. In Figure 10, we show the stellar mass distribution, adaptively smoothed and seen edge- and face-on, for the "iso-ism" model at (clockwise from upper left) T = 0.5 Gyr, T = 1.0 Gyr, T = 1.5 Gyr, and T = 2.0 Gyr. Gas in the inner parts of the halo quickly cools to roughly 10^4 K, settles into a thin, rotationally supported disk, and forms stars. The 10^4 K gas in the disk is highly compressible, obeying a nearly isothermal equation of state. Consequently, the self-gravitating gaseous disk becomes gravitationally unstable as soon as it reaches a moderate surface density. The Toomre (1964) instability quickly causes a fragmentation of the smooth gas disk into clumps, which collapse further under their own self-gravity and form stars on a short time-scale. As the galaxy ages, the stellar clumps coalesce through dynamical friction into ever larger lumps, destroying the disk. By $T = 2\,$Gyr, the stars are mainly confined in two large blobs, with numerous smaller clumps orbiting the center.

The evolution of the galaxy in the "iso-ism" model contrasts sharply with that in the corresponding "multiphase-ism" run. We illustrate this in in Figure 11. Again, the gas cools into a thin, star-forming disk. However, supernova feedback regulates the rate of star formation and the dynamics of the dense star-forming gas. Owing to feedback, the ISM is pressurized, stabilizing the gas against the Toomre instability. Consequently, a smooth distribution of gas is maintained in the plane of the disk and stars form steadily, increasing the size of the disk from $6h^{-1}\,$kpc at T = 0.5 Gyr to $> 12h^{-1}\,$kpc at $T = 2.0\,$Gyr. Since the gas remains stable and does not fragment into clumps, the disk largely avoids angular momentum loss and the simulation yields a large disk galaxy with only a modest bulge.

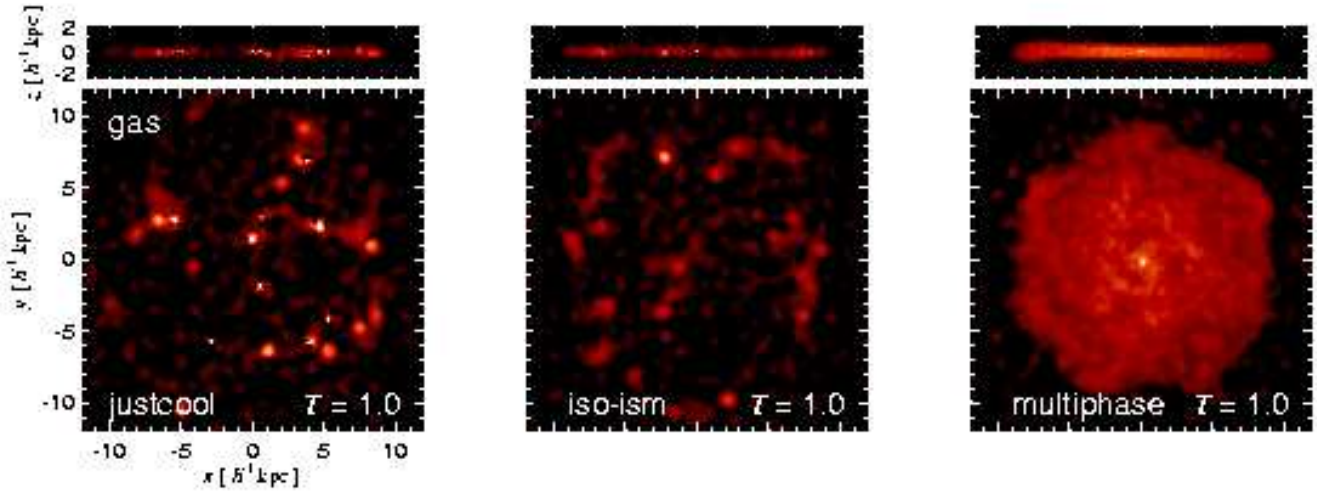

FIG. 12.— Comparison of the gas mass distribution in the "justcool" (left), "iso-ism" (center), and "multiphase-ism" (right) simulations at T = 1.0 Gyr. Both the "justcool" and "iso-ism" models produce gas disks fragmented by catastrophic Toomre instability. By contrast, the "multiphase-ism" model yields a stable disk supported by additional pressure supplied by the Springel & Hernquist (2003a) model for the ISM.

In Figure 12, we compare the gas mass distributions in the "justcool" (left), "iso-ism" (center), and "multiphase-ism" (right) simulations at T = 1.0 Gyr. Both the "justcool" and "iso-ism" models produce clumpy gas disks that fragmented by the Toomre instability. In fact, the time evolution of the "justcool" and "iso-ism" models is very similar, except that in the former case the instabilities occur earlier, showing that star formation can have a stabilizing effect by reducing the gas surface density. Note, however, that only the "multiphase-ism" model produces a gaseous disk that exhibits long-term stability.

In summary, our simulations of the formation of disks in isolated halos clearly show that the modeling of the ISM has a strong effect on disk stability. In particular, an isothermal equation of state for star-forming gas produces gaseous disks that are violently unstable. Under these conditions it would be difficult if not impossible to form large, extended disk galaxies unless the gas surface density is always kept extremely low, for example by adopting an unrealistically short star formation time-scale that would conflict with the observed Kennicutt law.

In contrast, the multiphase model for the ISM yields disk galaxies that are more stable. The stiffer equation of state produces disks that are more resilient against Toomre instability than in models with an effectively isothermal ISM. Fragmentation is avoided, enabling the steady formation of large stellar disks even when the disk is gas-rich and has a high gaseous surface density. Therefore, we suggest that the behavior of the equation of state in our multiphase description of the ISM is the primary reason why our cosmological simulation can produce disk galaxies with negligible bulge components. This conclusion should be insensitive to the detailed features of our multiphase model of the ISM, provided that the actual equation of state for star-forming gas behaves similarly to the one proposed by Springel & Hernquist (2003a).

7. CONCLUSIONS

We have performed a high-resolution cosmological simulation that included gas dynamics, radiative heating and cooling, and star formation and supernova feedback, modeled in the framework of a subresolution description of a multiphase ISM. Inspecting the ten largest halos, we identified a well-resolved disk galaxy at redshift z = 0. The disk galaxy has realistic photometric properties, including a reasonable central surface brightness and exhibits good agreement with the I-band Tully-Fisher relation. Most important, this object is the first published example of a disk galaxy from a simulation that features a simple exponential surface brightness profile without having a large bulge component. Our work demonstrates that extended disk galaxies can form in a ΛCDM cosmology within full hydrodynamic simulations, an important step forward in understanding the origin of disk galaxies.

While the total angular momentum of the stellar component of the disk galaxy is appropriate for observed galaxies with similar rotation velocities, the inner regions of the galaxy have low specific stellar angular momentum. It is not clear whether this is a problem with the physics, e.g. excessive angular momentum loss by the gas, or is at least partly an artifact of our inability to completely resolve the thin stellar disk. The disk galaxy in our simulation does not have an obvious problem with its radial size, but statistical studies with samples of simulated disk galaxies will be needed to settle this question. However, we find the success achieved here encouraging and suggest that the problem with disk size is alleviated by employing equations of state for star-forming gas that are stiffer than isothermal.

Using a suite of isolated galaxy formation simulations, we have explicitly demonstrated the consequences our treatment for the ISM has on the formation of disk galaxies. Simulations with an effectively isothermal ISM yield gravitationally unstable disks and fail to produce large, smooth stellar disks. In contrast, the multiphase model supplies enough pressure support to the star-forming gas to prevent catastrophic Toomre instability, allowing stable galactic disks to form. We have also verified that these conclusions do not depend on details of our numerical integration.

Our work differs in a number of respects from earlier numerical attempts to study disk galaxy formation. We have used a novel formulation of smoothed particle hydrodynamics that, by construction, conserves both energy and entropy si-

multaneously, even when smoothing lengths vary in response to changes in density (Springel & Hernquist 2002). While we consider it unlikely that previous numerical work on galaxy formation with SPH was strongly affected by inaccuracies in e.g. entropy conservation, it is clearly preferable to use a fully conservative scheme that mitigates against any numerical "overcooling."

More important, we have formulated the consequences of feedback using a subresolution model for star formation in a multiphase ISM. In this scheme, the local supernova feedback modifies the effective equation of state for star-forming gas, leading to an efficient self-regulation of star formation and a stabilizing effect on highly overdense gas. This aspect of our modeling feeds directly into the dynamics of forming disks by modifying the pressure gradient term in the hydrodynamic equations of motion.

Our formulation of the ISM physics has a number of advantages over earlier treatments of star formation and feedback. Other workers have implemented techniques to allow feedback to have a significant dynamical impact by, e.g. depositing thermal energy into gas surrounding star-forming regions and artificially delaying the radiative loss of this energy by the gas for an ad hoc time interval. While similar in spirit to our method, these approaches make the comparison of results from different calculations challenging because the consequences of feedback are difficult to summarize in a concise, quantitative form. When expressed in terms of an effective equation of state, as done here, the dynamical implications of feedback become easier to interpret. A discussion in terms of the effective equation of state is also relatively insensitive to the detailed physics responsible for pressurizing the gas, and enables one to relate the description of feedback to observations of the ISM.

In order to demonstrate the sensitivity of galaxy formation to the physics of star-forming gas, we employed a simple multiphase model of the ISM (Springel & Hernquist 2003a), where the gas is imagined to be thermally unstable at sufficiently high densities and exists in two distinct phases, in pressure equilibrium. In detail, it is not plausible that this is a true picture of the ISM of disk galaxies, because this model ignores, e.g. turbulent motion, magnetic fields, and cosmic rays. However, we believe that the basic points of our modeling do not depend on these complications. The evolution of the different models shown in § 6 depends mainly on the effective equation of state for the star-forming gas on scales which characterize the Toomre instability. According to the Toomre criterion, a thin sheet of gas in differential rotation will be gravitationally unstable if

$$Q \equiv \frac{c_s \kappa}{\pi G \Sigma} < 1\,, \tag{10}$$

where c_s is the sound speed, κ is the epicyclic frequency, and Σ is the surface density. In terms of an effective temperature of the gas,

$$Q \approx 1.1\, T_5^{1/2}\, \kappa_{35}\, \Sigma_{75}^{-1}\,, \tag{11}$$

where $\kappa_{35} \equiv \kappa/(35\,\mathrm{km\,sec^{-1}kpc^{-1}})$ and $\Sigma_{75} \equiv \Sigma/(75\,\mathrm{M_\odot\,pc^{-2}})$ are values characteristic of the Milky Way in the solar neighborhood, and $T_5 \equiv T/(10^5\,\mathrm{K})$. If the gas obeyed an isothermal equation of state with $T_5 = 0.1$, then $Q \sim 0.3$, and the disk would be violently unstable, as for example in the case of our "iso-ism" simulations described in § 6. With our equation of state, however, the effective temperature at densities characteristic of a forming galaxy would be $T_5 \sim 1$ (see Fig. 1 of Springel & Hernquist 2003a), so $Q > 1$ and the disk would be stable, explaining why our "multiphase-ism" models in § 6 produce realistic disks. Moreover, for thin disks of gas, the fastest growing unstable mode has a wavelength which is a significant fraction of the disk size (e.g. Binney & Tremaine 1987) and, therefore, the growth of the instability is sensitive only to the macroscopic equation of state for the ISM. Whether or not the effective equation of state we have adopted (i.e. Figure 1) for the ISM is appropriate in detail is uncertain, but this question is largely independent of the exact properties of star-forming gas. In particular, we expect our results to generalize to other models for the ISM with similar effective equations of state.

Having identified one exponential disk galaxy in our simulation, future work is needed to extend our analysis to other galaxies. For example, a good statistical sample of simulated disks is needed before we can characterize the distribution of disk sizes and their morphological types, as well as the photometric and kinematic properties of the galaxies. This work will require larger simulations of substantial dynamic range in order to obtain adequate numbers of simulated disk galaxies, but we find the initial successes described here and recently by other authors highly encouraging. A comparison with the wealth of observational data on the structural parameters of galaxies in the local universe will then show whether hydrodynamical simulations are finally producing realistic disk galaxies.

This work was supported in part by NSF grants ACI 96-19019, AST 98-02568, AST 99-00877, AST 00-71019, and AST-0206299, and NASA ATP grants NAG5-12140, NAG5-13292, and NAG5-13381. NY acknowledges support from JSPS Special Research Fellowship (02674). The simulations were performed at the Center for Parallel Astrophysical Computing at the Harvard-Smithsonian Center for Astrophysics.

REFERENCES

Abadi, M. G., Navarro, J. F., Steinmetz, M., & Eke, V. R. 2003a, ApJ, 591, 499
—. 2003b, ApJ, 597, 21
Binney, J. & Tremaine, S. 1987, Galactic Dynamics, Princeton University Press
Contardo, G., Steinmetz, M., & Fritze-v. Alvensleben, U. 1998, ApJ, 507, 497
Courteau, S. 1997, AJ, 114, 2402
Cousins, A. W. J. 1978, Monthly Notes of the Astronomical Society of South Africa, 37, 8
Davé, R., Hernquist, L., Katz, N. & Weinberg, D.H. 1999, ApJ, 511, 521
Freeman, K. C. 1970, ApJ, 160, 811
Fukugita, M., Ichikawa, T., Gunn, J. E., Doi, M., Shimasaku, K., & Schneider, D. P. 1996, AJ, 111, 1748
Giovanelli, R., Haynes, M. P., Herter, T., Vogt, N. P., Wegner, G., Salzer, J. J., da Costa, L. N., & Freudling, W. 1997, AJ, 113, 22
Governato, F., et al. 2002, preprint (astro-ph/0207044)
Han, M., & Mould, J. R. 1992, ApJ, 396, 453
Hernquist, L. 1993, ApJ, 404, 717
Hernquist, L. & Springel, V. 2003, MNRAS, 341, 1253
Hultman, J. & Pharasyn, A. 1999, A&A, 347, 769
Johnson, H. L., & Morgan, W. W. 1953, ApJ, 117, 313
Katz, N. 1992, ApJ, 391, 502
Katz, N., & Gunn, J. E. 1991, ApJ, 377, 365
Katz, N., Weinberg, D.H. & Hernquist, L. 1996, ApJS, 105, 19
Kauffmann, G., et al. 2003, MNRAS, 341, 33
Kennicutt, R. C. 1989, ApJ, 344, 685
—. 1998, ApJ, 498, 541
Kroupa, P. 2001, MNRAS, 322, 231
Martin, C. L., & Kennicutt, R. C. 2001, ApJ, 555, 301
Mathewson, D. S., Ford, V. L., & Buchhorn, M. 1992, ApJS, 81, 413
McKee, C. F., & Ostriker, J. P. 1977, ApJ, 218, 148
Mo, H. J., Mao, S., & White, S. D. M. 1998, MNRAS, 295, 319
Nagamine, K., Springel, V., & Hernquist, L. 2003a, MNRAS, accepted (astro-ph/0302187)
—. 2003b, MNRAS, accepted (astro-ph/0305409)
Nagamine, K., Cen, R., Hernquist, L., Ostriker, J.P. & Springel, V. 2003c, ApJ, submitted (astro-ph/0311294)
Nagamine, K., Springel, V., Hernquist, L. & Machacek, M. 2003d, MNRAS, submitted (astro-ph/0311295)
Navarro, J. F. 1998, preprint (astro-ph/9807084)
Navarro, J. F., & Benz, W. 1991, ApJ, 380, 320
Navarro, J. F., Frenk, C. S., & White, S. D. M. 1995, MNRAS, 275, 56
Navarro, J. F., & Steinmetz, M. 1997, ApJ, 478, 13
—. 2000, ApJ, 538, 477
Navarro, J. F., & White, S. D. M. 1993, MNRAS, 265, 271
—. 1994, MNRAS, 267, 401
O'Shea, B.W., Nagamine, K., Springel, V., Hernquist, L. & Norman, M.L. 2003, ApJ, submitted (astro-ph/0312651)
Power, C., Navarro, J. F., Jenkins, A., Frenk, C. S., White, S. D. M., Springel, V., Stadel, J., & Quinn, T. 2003, MNRAS, 338, 14
Sommer-Larsen, J., & Dolgov, A. 2001, ApJ, 551, 608
Sommer-Larsen, J., Götz, M., & Portinari, L. 2002, Ap&SS, 281, 519
—. 2003, ApJ, 596, 47
Sommer-Larsen, J., Gelato, S., & Vedel, H. 1999, ApJ, 519, 501
Springel, V., & Hernquist, L. 2002, MNRAS, 333, 649
—. 2003a, MNRAS, 339, 289
—. 2003b, MNRAS, 339, 312 (for an updated version, see astro-ph/0206395)
Steinmetz, M., & Müller, E. 1994, A&A, 281, L97
Steinmetz, M., & Müller, E. 1995, MNRAS, 276, 549
Steinmetz, M., & Navarro, J. F. 1999, ApJ, 513, 555
Toomre, A. 1964, ApJ, 139, 1217
Tormen, G. 1997, MNRAS, 290, 411
Yepes, G., Kates, R., Khoklov, A. & Klypin, A. 1997, MNRAS, 284, 235